Giant reduction of thermal conductivity in twinning superlattice InAsSb nanowires

Lorenzo Peri[1, †, ¶], Domenic Prete[1, ¶], Valeria Demontis[1], Valentina Zannier[1], Francesca Rossi[2], Lucia Sorba[1], Fabio Beltram[1] and Francesco Rossella[1,3, *]

[1] NEST, Scuola Normale Superiore and Istituto Nanoscienze-CNR, Pisa, Italy
[2] IMEM-CNR, Parco Area delle Scienze 37/A, I-43010 Parma, Italy
[3] Dipartimento di Scienze Fisiche, Informatiche e Matematiche, Università di Modena e Reggio Emilia, Modena, Italy
[†] Present address: Yusuf Hamied Department of Chemistry, Lensfield Road, Cambridge, CB2 1EW, United Kingdom
[¶] equally contributing author
[*] Corresponding author

Keywords: Thermal Conductivity, Twinning Superlattice Nanowires, Thermoelectricity, 3ω-method, ZT

ABSTRACT
Semiconductor nanostructures hold great promise for high-efficiency waste-heat recovery exploiting thermoelectric energy conversion. They could significantly contribute to the implementation of environmentally friendly energy sources and to the realization of self-powered biomedical wearable devices. A crucial thermoelectric material requirement is a reduced thermal conductivity together with good electrical transport properties.
In this work we demonstrate a drastic reduction of the thermal conductivity in III-V semiconductor nanowires as a result of the introduction of periodic crystal-lattice twin planes during growth. The electrical and thermal transport of these nanostructures, known as twinning superlattice nanowires, are probed and compared with their twin-free counterparts, showing a one order of magnitude decrease of thermal conductivity while maintaining unaltered electrical-transport properties and Seebeck coefficients. This leads to tenfold enhancement of the thermoelectric figure of merit, ZT. Our study reports for the first time the complete experimental measurement of electrical and thermal properties in twinning superlattice nanowires, demonstrating their emergence as a novel class of nanomaterials of great potential for high-efficiency thermoelectric-energy harvesting.

INTRODUCTION

The urgent need for locally available, non-intermittent energy sources to power of wearable, implantable and biomedical devices has recently boosted theoretical and experimental studies on thermoelectric energy conversion [1], which entails the generation of an electrical current or voltage from a temperature gradient, leading to conversion of potentially wasted heat into usable electrical energy. A good thermoelectric material should possess high electrical conductivity, to facilitate the flow of charge carriers (e.g., electrons), together with low thermal conductivity, to minimize irreversible flow of heat [2]. In the context of the Onsager-de Groot-Callen model [3], the performance at the temperature T of a thermoelectric material can be quantified with the thermoelectric figure of merit $ZT = \frac{\sigma S_e^2 T}{\kappa}$, where σ and κ are the electrical and thermal conductivities, respectively, and S_e is the electronic Seebeck coefficient of the material [4-5]. Striving to achieve higher figures of merit, research efforts have mainly focused on different ways to enhance electrical conductivity [6]. However, it is evident from the formula of ZT that another way to optimize ZT is to reduce the thermal conductivity - usually dominated by the lattice contribution in semiconductors at room temperature - without impacting the electrical transport properties.
In this frame, semiconductor nanowires (NWs) are extremely promising [7-12], as their high aspect ratio leads to an increase of phonon scattering at the lateral boundaries of the nanostructure. This effect, known as the Casimir effect, leads to a strong reduction of the effective phonon mean free path with respect to the intrinsic value of the bulk material [13], yielding to an effective reduction of the thermal conductivity

[14-16]. For instance, InAs NWs - usually grown with a wurtzite (WZ) crystal structure - have been widely studied for thermoelectric applications [17,18]. Unfortunately, despite the Casimir effect, single crystal nanowires made of common III-V or IV semiconductors still cannot compete with the industry standard thermoelectric materials (e.g. Bi_2Te_3) because their figure of merit is still significantly lower (between one and two orders of magnitude [19]) than the state of art thermoelectric materials employed in thermoelectric generators.

Improvement is still possible in III-V semiconducting nanowires by employing polytypic structures known as twin superlattices (TSLs) [20-25]. These structures involve the periodic repetition of twin planes, i.e., stacking faults inducing a rotation of the orientation of the crystal lattice with respect to the lattice portion preceding it along the NW growth direction [26]. The crystal structure around a twin plane can also be seen as an inclusion of a different polytype with respect to the dominant one, such as a wurtzite (WZ) segment in a zincblende (ZB) structure [27]. The random occurrence of this kind of stacking faults is often observed in vapor liquid solid (VLS)-grown III-V NWs and is usually considered as a defect, since they can have detrimental effects on the electrical properties of the material [28]. On the other hand, the intentional introduction of these planar defects in a periodic fashion to form a crystal phase superlattice [29] can controllably modify the electronic band structure of the material, e.g., promoting the formation of electronic minibands [30]. The periodic repetition of twin planes in TSL NWs can be achieved by finely tuning the growth parameters, the NW diameter and by the introduction of a controlled amount of impurities [31-32].

In this work, we experimentally investigate $InAs_{1-x}Sb_x$ NWs as novel nanomaterials for the realization of next-generation thermoelectric energy converters. A small and controlled amount of Sb added to InAs NWs changes the crystal structure from pure WZ to pure ZB, via intermediate stacking-faults and periodic-twinning regimes [31, 33] and these nanostructures are excellent candidates to feature strongly reduced thermal conductivity [34-35] with unaffected electrical conductivity [30,36]. For the first time, we experimentally demonstrate that periodic twinning in semiconductor nanowires allows to engineer heat transport inside the material to achieve a drastic decrease of its thermal conductivity together with unaffected electrical conductivity, hence improving its thermoelectric properties. We have measured the electrical and thermal transport properties of TSL InAsSb NWs with different twin plane periodicity and compared them with those of pure WZ InAs NWs. We also compared the properties of TSL InAsSb NWs with their untwinned InAsSb counterparts, addressing the relative effect of the incorporation of Sb atoms in the crystal lattice and of the formation of twin planes in the nanostructure. We shall show a strongly improved thermoelectric figure of merit, calculated by exploiting Mott's formula [37] and direct measurements for the estimation of the Seebeck coefficient. We believe that this work paves the way for the development of high-performance thermoelectric generators based on III-V semiconductor nanostructures and may give new life to the research on phonon engineering in semiconducting nanomaterials.

RESULTS & DISCUSSION

Twinning Superlattice Nanowires

The nanowire samples grown for the present study include WZ InAs NWs, ZB InAsSb NWs and TSL InAsSb NWs. High resolution TEM (HRTEM) images of the different InAsSb NWs are reported in **Figure 1**, while **Table 1** reports the growth conditions employed to achieve the different nanostructures. Figure 1 (a-d) shows the HRTEM images of the TSL NWs (samples A, B, C, D of Table 1). Their structural and morphological properties were compared with pure ZB InAsSb NW (sample E; zoomed HRTEM in Figure 1(e)). The crystal structure is WZ in the InAs NW stem grown before the InAsSb segment, but it changes to ZB as soon as some Sb is incorporated, as already reported elsewhere [33, 38]. This can be ascribed either to the role of Sb as a surfactant - changing the stable facet structure - or to the much stronger affinity of Sb to the Au seed particle relative to As - which dramatically affects the actual V/III ratio at the growth front and the particle contact angle. Simultaneously, there is a non-negligible lateral growth occurring together with the axial elongation during the InAsSb segment growth, so that the final NW diameter is larger than the

nanoparticle (NP) size. NWs with Sb fraction higher than 7% (sample E in Table 1) have a pure ZB crystal structure without any structural defect, while samples with Sb fraction in the range between 1% and 6% (A-D in the table) show a periodic repetition of twin planes for the whole length, making them TSL NWs. In fact, the incorporation of small amounts of Sb during growth and the formation of twin planes are intrinsically entangled. Most importantly, we found that the twin periodicity is affected by both chemical composition (Sb fraction) and diameter of the gold NP used for the VLS growth. In particular, for the same NP diameter, the periodicity can be increased by increasing the Sb fraction. In turn, larger NPs yield TSL NWs with longer twin periodicity. However, it should be noticed that the NP diameter has a more drastic effect, in fact comparing NWs with a similar variation of Sb fraction, when the NP diameter is fixed the periodicity changes by a factor 1.5 (samples C and B), while changing the NP diameter results in a periodicity change of a factor ~ 9 (samples D and A). This trend is consistent with what is reported for different materials [27, 28] and explained with the distortion of the nanoparticle in response to the evolution of the hexagonal cross-section of NWs with non-parallel {111} side faces during the growth [27]. Phonon scattering occurring at the twin planes (pictorially represented in Figure 1(f)-bottom right panel) is expected to drastically reduce the thermal conductivity while preserving the electrical conduction at room temperature. The formation of TSL is indeed associated to the onset of peculiar features in the band structure of the semiconductor, known as minibands, originating by the folding of the electron dispersion relation due to the added periodicity [30]. Electronic minibands allow the electrons to undergo easy tunnelling and leave the electrical current unperturbed. The phononic dispersion, however, is different before and after the twin planes, and the elastic deformation wave is partially reflected at the interface between the two twinned crystal structures [39]. This results in an additional thermal resistance at the interface, known as Kapitza resistance [40], due to imperfect phonon matching. Each twin plane contributes to increase the thermal resistance, yielding to a strong decrease of the thermal conductivity of the entire nanostructure.

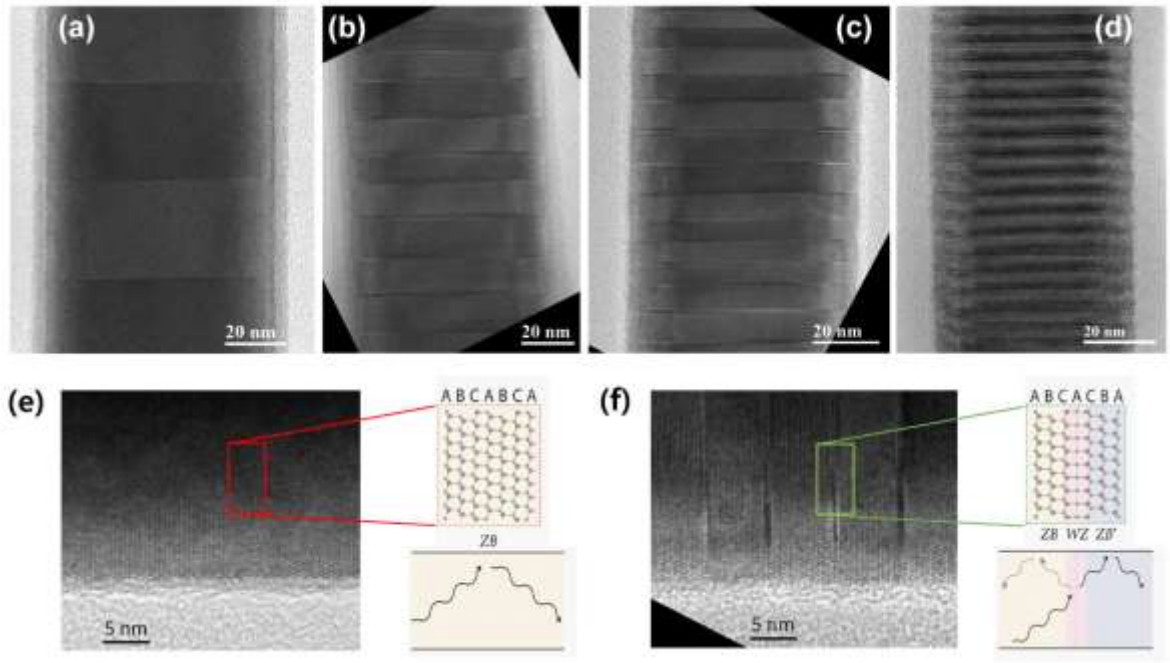

Figure1. HRTEM images of a portion of the InAsSb NWs of samples A (a), B (b), C (c), D (d), with Sb fraction respectively 5.8%, 2.1%, 1.6% and 5.2%. The diameter for the gold catalyzer nanoparticle is 40 nm for samples A, B, C and 20 nm for sample D. The different twin periodicity is clearly seen thanks to the image contrast. Magnified HRTEM image and ball-stick representation of a pure ZB (e) and a TSL (f) InAsSb NW (sample C). The ball-and-stick representations highlight the difference between the crystal stacking order in the ZB phase (ABCABCA) and in the TSL (ABCACBA). In the lower right corner of each panel there is a schematic depiction of phonon scattering in the two different crystal structures: only boundary scattering in the pure ZB NW, with additional scattering at the twin planes in the TSL NW.

Sample	Au NP diameter (nm)	TBAs line pressure (Torr)	TDMASb line pressure (Torr)	NW average diameter (nm)	$InAs_{(1-x)}Sb_{(x)}$ composition (Sb fraction: x)	Crystal structure (twin periodicity)
A	40	1.4	0.3	80 ± 10	0.058	Twinned (30 nm)
B	40	1.6	0.2	80 ± 10	0.021	Twinned (12 nm)
C	40	1.6	0.1	70 ± 10	0.016	Twinned (8 nm)
D	20	1.5	0.2	60 ± 10	0.052	Twinned (3.5 nm)
E	20	1.5	0.4	70 ± 10	0.072	Pure ZB
F	60	3	0	70 ± 10	0	WZ

Table 1: Growth parameters and resulting compositional, morphological and structural properties of the NWs measured in the present work.

Thermal transport properties

Direct measurements of the thermal transport properties of TSL InAsSb NWs were performed focusing on two different samples among the different grow batches, namely samples C and D that exhibit twin periodicity of 8 nm and 3.5 nm, respectively. The performance of these NWs was compared to that of pure ZB InAsSb NWs (sample E) and that of WZ InAs NWs (sample F). Single NW devices were realized implementing four-electrode architectures in suspended nanowires, specifically designed to perform thermal conductivity measurements via the 3ω method [41-43], an electrical technique exploiting self-heating and non-linear effects for the measurement of the thermal conductivity in high aspect-ratio nanostructures. These devices implement a nanowire suspended at approximately 250 nm from the substrate, as visible in the scanning electron micrograph reported in **Figure 2(a)**. This allows to decouple the nanostructure from the substrate and avoid any heat loss that may detrimentally affect the thermal conductivity measurement. The 3ω method resorts on the measurement of the third harmonic of the voltage drop, $V_{3\omega}$, in the semiconducting nanowire fed with an AC current at frequency omega, I_{ω}. The details on the experimental setup used for implementing the 3ω-method can be found in the Methods section. Figure 2(b-c-d) reports three examples of measured $V_{3\omega}$ signals as function of I_{ω} for pure ZB InAsSb NWs (sample E), TSL InAsSb NWs with 3.5 nm (sample D), and TSL InAsSb NWs with 8 nm period (sample C). Together with the cubic fit based on the simplified analytical model [43], we resorted to finite element modeling to exactly solve the temperature and voltage profile in the nanostructure and achieve a precise fit to our experimental data (Supporting Information SI.1). Figures 2(e) and (f) report a comparison between the fit outcomes, revealing the limitations of the purely analytical model which are overcome by employing finite element analysis.

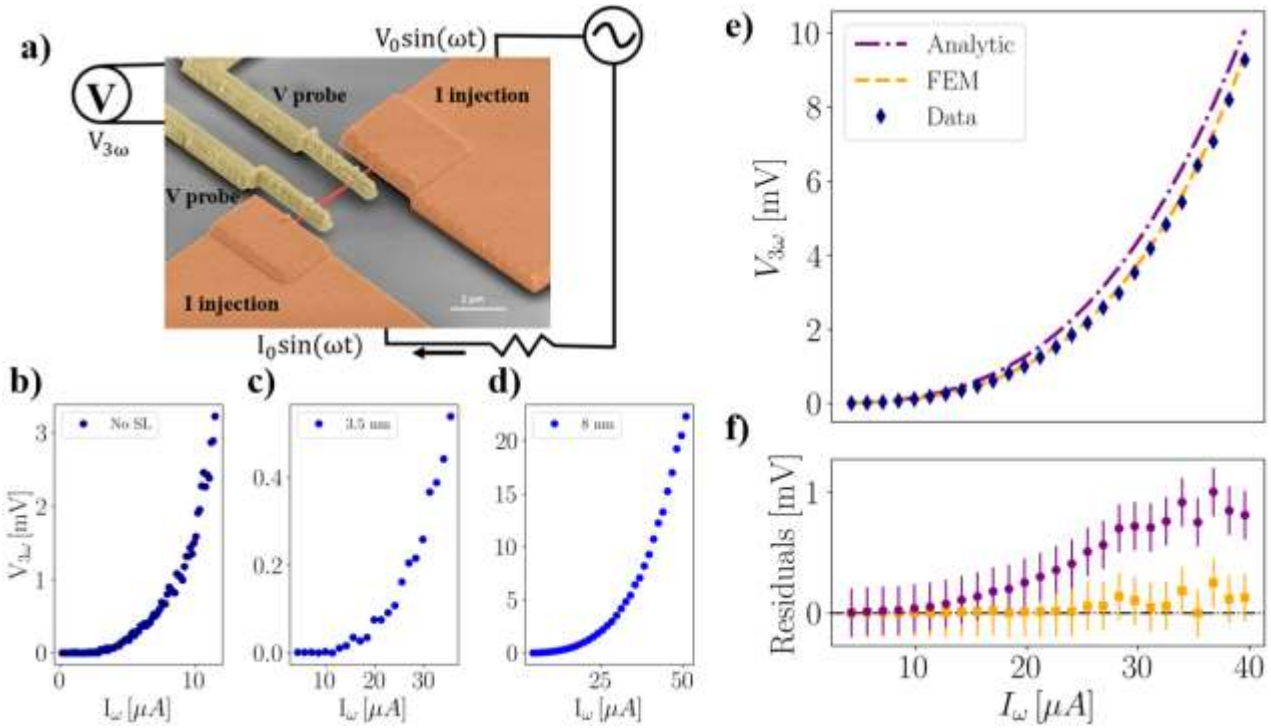

Figure 2. (a) SEM image and circuital scheme of a typical NW-based device for thermal conductivity measurements with the 3ω method. In false colors are highlighted the suspended NW (red), the injection electrodes (orange) which also act as a thermal anchor, and the pick-up electrodes (yellow) for a 4-wire measurement of $V_{3\omega}$ with a Lock-In amplifier. 100 K Ω resistor was used to inject the current. Experimental $V_{3\omega} - I_\omega$ curves measured for pure ZB InAsSb NWs (b), TSL InAsSb NWs with 3.5 nm period (c) and with 8 nm diameter (d). (e) An example of a measured $V_{3\omega}$ vs I_ω curve and the relative fit performed via finite elements analysis compared with the fit performed by employing the analytical formula. (f) Fit residuals for the analytical model and the fit resulting from the numerical calculations. For higher values of I, the analytical model deviates from the experimental data, differently from the results of the finite element modeling which show negligible deviation.

The resulting thermal conductivities are reported in **Figure 3** and show a marked reduction of κ in the InAsSb NWs and particularly in TSL InAsSb NWs. Seven independent campaigns of measurements were carried out and the results correspond to the different groups of experimental points reported in Figure 3(a). The thermal conductivity for the WZ InAs NWs (average diameter 70 nm) is found to be $14 \pm 6 \frac{\mathrm{W}}{\mathrm{mK}}$. Notably, while fluctuations in the reported values of *k* occur due to manifold reasons, including suboptimal device fabrication, the impact of different measurement campaigns and of device exposure to air, the reported average value of *k* is in very good agreement with previous experimental and theoretical results [7,17,41,44]. A decrease of κ is observed in the pure ZB InAsSb NWs, with measured values ranging from $6.3 \pm 2.9\ \mathrm{W/mK}$ to $5.4 \pm 2.8\ \mathrm{W/mK}$ for sample E. This is consistent with the effect on thermal transport of the introduction of Sb in other III-V semiconductor alloys, as reported elsewhere [45] and predicted by the Klemens-Drabble theory (ultimately stemming from the heavier mass of Sb atoms with respect to As atoms). A further reduction is observed in the TSL InAsSb NWs**,** despite the lower Sb content. The InAsSb NWs with 8 nm twinning period (sample C) exhibit a thermal conductivity ranging from $3.4 \pm 1.4\ \mathrm{W/mK}$ to $2.8 \pm 1.3\ \mathrm{W/mK}$. The lowest κ was measured for TSL InAsSb NWs with twinning period of 3.5nm (sample D), with an average value of $1.2 \pm 0.6\ \mathrm{W/mK}$. It is worth noting that the uncertainties reported for our results obtained with the 3ω technique are fully consistent with the uncertainties reported in literature also employing different methods [7,41,46]. In the present case, the uncertainty in the reported value of *k* is generated by error propagation theory applied to the multiple experimental parameters entering the measure of *k*, namely the distance between the electrodes, the NW cross section, the NW electrical resistance and its temperature coefficient. Overall, we ascribe the observed experimental results to the enhanced phonon scattering caused by the incorporation of Sb and by the occurrence of twin planes, with the latter having a stronger impact. In fact, on the one hand the observed reductions of κ in ZB InAsSb NWs

with respect to WZ InAs NWs cannot be attributed to the change in crystal structure form WZ to ZB. Indeed, the opposite effect – increase of thermal conductivity - was reported for pure ZB InAs NWs with respect to pure WZ ones [44]. On the other hand, the observed reduction in κ could in principle be ascribable to the slight differences between the diameters of the measured NWs, according to the functional dependence expressed by the Ziman's formula [7] which describes how the κ of the nanowire deviates from the κ of the bulk material as an effect of its diameter:

$$\kappa_{NW} = \kappa_{Bulk}\left(1 - e^{-D/\Lambda_i}\right) \quad (1)$$

where D is the NW diameter and Λ_i the phonon mean free path due to internal scattering, which is equal to 250 nm in WZ InAs [7]

To rule out this scenario and take into account the role of the NW diameter, we defined a normalized κ, $\kappa_{norm} = \kappa_{NW}/\kappa_{InAs}$, where κ_{NW} is the value of the thermal conductivity measured in the InAsSb NW, while κ_{InAs} is the thermal conductivity of an InAs nanowire with the same diameter. The dimensionless parameterκ_{norm} can be regarded as an estimate of the effective reduction in thermal transport efficiency occurring in our nanostructures. κ_{norm} obtained in our samples are reported in Figure 3(b). κ_{norm}=1 by definition for sample F (70 nm diameter WZ InAs NWs)κ_{norm} =0.55 ± 0.19 in pure ZB InAsSb NW (sample E), $0.14 \pm 0.06$$0.11 \pm 0.04$for the TSL InAsSb NWs with 8 nm (sample) and 3.5 nm (sample D) twinning period, respectively. In other words, this indicates a nine-fold reduction in thermal conductivity for a TSL InAsSb NW with 3.5 nm twinning period with respect to a WZ InAs NW with the same diameter. Interestingly, the incorporation Sb in a fraction of 7% in InAsSb NWs is responsible for a reduction of the thermal conductivity of a factor ~2, while a stronger effect is coming from the presence of the twin planes in the twinned samples, up to a further factor ~5 difference between untwinned InAsSb NWs and twinned (but with less Sb concentration) InAsSb NWs with 3.5 nm twin period. Therefore, even if both Sb incorporation and the presence of twin planes are found to be responsible for the reduction of the thermal conductivity, the latter appears to have a much stronger impact and is thus to be investigated for the optimization of novel thermoelectric nanomaterials. We tentatively quantify the different impact of the two parameters with a contribution ratio of ~5/2.

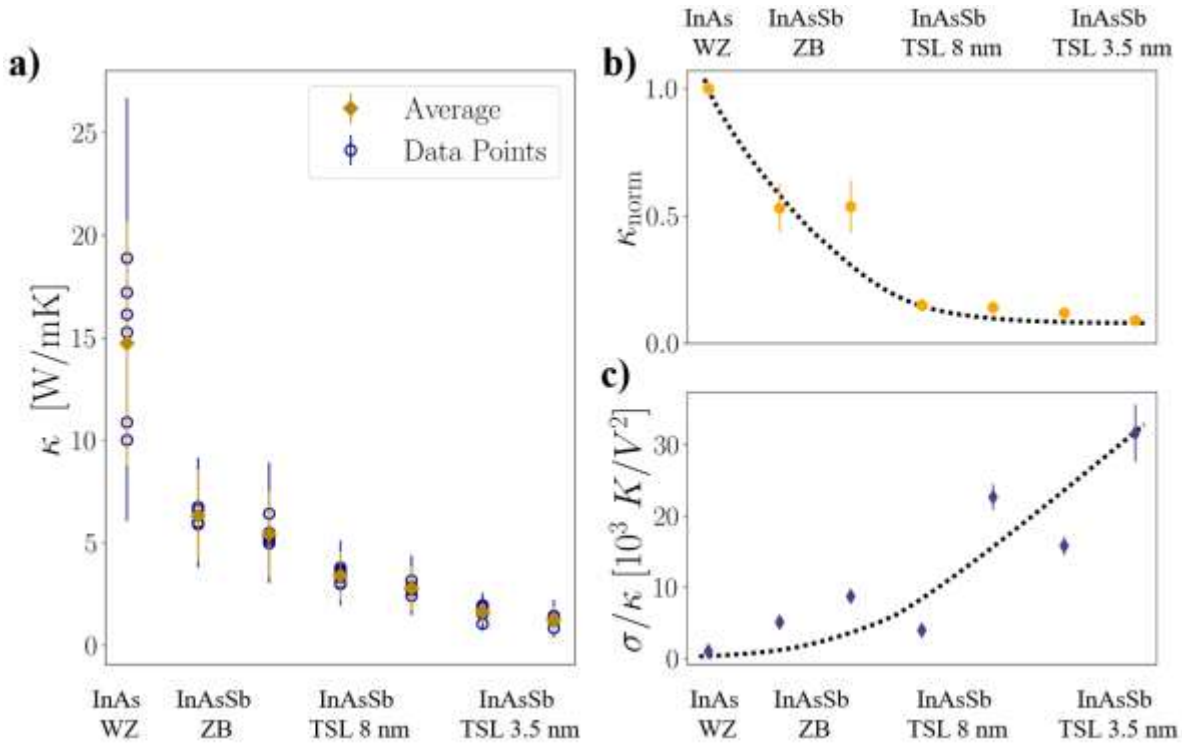

Figure 3: (a) Measured thermal conductivity κ for the NWs with different crystal structure. Each group of experimental points correspond to an independent campaign of measurements. (b) Thermal conductivity normalized with respect to the value of a 70 nm diameter WZ InAs NW, accounting for the different diameters of the measured NW-based devices. (c) Measured ratio of

electrical and thermal conductivity for the different devices, indicating a strong increase in the ratio σ/κ which appears directly in the thermoelectric figure of merit. Dashed lines in panels (b) and (c) are guides to the eye.

Electrical and Thermoelectric transport properties

Together with drastically reduced thermal conductivity, the peculiar polytypic InAsSb heterostructure studied in this work also displays excellent electrical transport properties, equivalent to those of their pure ZB and WZ counterparts. This was verified by realizing conventional NW-based field effect transistors (FETs) with the nanostructure laying on a substrate. Here, the nanowires are drop-casted onto a SiO2/Si++ substrate to perform field effect electrical measurement in standard back-gate configuration (Supporting Information SI.2). We fabricated several NW-based FETs starting from sample D (TSL with 3.5 nm period), sample E (pure ZB) and sample F (WZ InAs) in order to measure their electrical transport properties, including the electrical conductivity, σ. This allowed us to extract the ratio σ/κ, a key parameter in thermoelectric applications which highlights the impact of the reduced thermal conductivity observed in our samples. Figure3(c) reports the σ/κ ratio for every measured NW sample, revealing an increase of σ/κ by one order of magnitude for the best performing TSL InAsSb NWs with respect to the WZ InAs NWs

Starting from the fabricated NW FETs we also measured, at room temperature, the current vs. back gate voltage characteristics, $I_{DS}(V_{GS})$ for NWs from samples D and E. For each device, from the slope of the linear region of the $I_{DS}(V_{GS})$ curve we obtained the transconductance $m_{lr} = dI_{DS}/dV_{GS}$ that allowed us to extract the electron mobility, μ [47] (supporting Information SI.3). **Figure 4(a)** reports the electrical mobility measured in all the FETs fabricated with NWs from sample E (ZB InAsSb NWs, blue dots) and sample D (TSL InAsSb NWs with 3.5 nm twinning period, red dots), as function of the electrical conductivity. Electrical mobility represents the key microscopic parameter quantifying the quality of the electrical transport in the NW-based device, while other parameters (such as the electrical conductivity) can be modulated by an external stimulus such as an applied back-gate voltage in a FET architecture. The results clearly indicate the similarity in electrical transport between pure ZB and TSL InAsSb NWs, with average electron mobility for both materials of approximately $1500\ cm^2/Vs$, also in agreement with the values reported in literature for nominally undoped WZ InAs NWs of similar diameter at room temperature [17, 47].

Finally we verified that our TSL InAsSb nanowires exhibit a Seebeck coefficient, S_e, practically indistinguishable from those exhibited by their untwinned counterparts as well as by WZ InAs NWs. To this aim we extracted S_e either by exploiting only analytical formulas (Sample E) or by using both direct measurements and calculations (Sample D), as described in detail in the Supporting Information (SI. 4), finding good agreement between the calculated and experimental data. This brings us to demonstrate a ZT for sample D (3.5 nm period TSL InAsSb NWs) exceeding of more than one order of magnitude the ZT displayed by WZ InAs NWs. Figure 4(b) displays the extracted Seebeck coefficient, S_e, as function of σ for pure ZB InAsSb NWs (sample E), for TSL InAsSb NWs with twinning period 3.5 nm (sample D) and for WZ InAs NWs (sample F): also in this case, as for the electron mobility of samples D and E, the similarity between the different nanostructures is quite evident. The spread observed in the measured values of μ, σ and S_e can be ascribed to the impact of different nanowire diameters (e.g. 20 nm spread for both twinned and untwinned NW batches) and to fabrication-related factors, e.g., slightly device-dependent contact resistances. Combining the measured thermal and electrical conductivity and the Seebeck coefficient, we extract the thermoelectric figure of merit, ZT, of the measured nanostructures, as reported in Figure 4(c). ZT values observed for WZ InAs NWs are in the range of 0.01-0.02, in good agreement with the values directly reported in literature or that can be extracted by combining results for thermal conductivity and power factor [17,18,41,44] , with ZT typically ranging from 0.01 to 0.04. We observe a first improvement for pure ZB InAsSb NWs, with a maximum value of $ZT = 0.042 \pm 0.003$, and a much stronger improvement for TSL InAsSb NWs, with highest reported $ZT = 0.24 \pm 0.07$ in III-V NWs, that is, a net increase in ZT exceeding an order of magnitude with respect to WZ InAs NWs with the same diameter. It is worth mentioning that this increase is achieved by acting solely on the thermal conductivity, while the electrical properties of TSL NWs are unaffected when compared to their untwinned counterparts. A further increase in ZT could be targeted by exploiting the several techniques reported in literature to optimizing separately

and independently the thermoelectric power, e.g., resorting to chemical doping or field effect control of the electrical conductivity [6, 17].

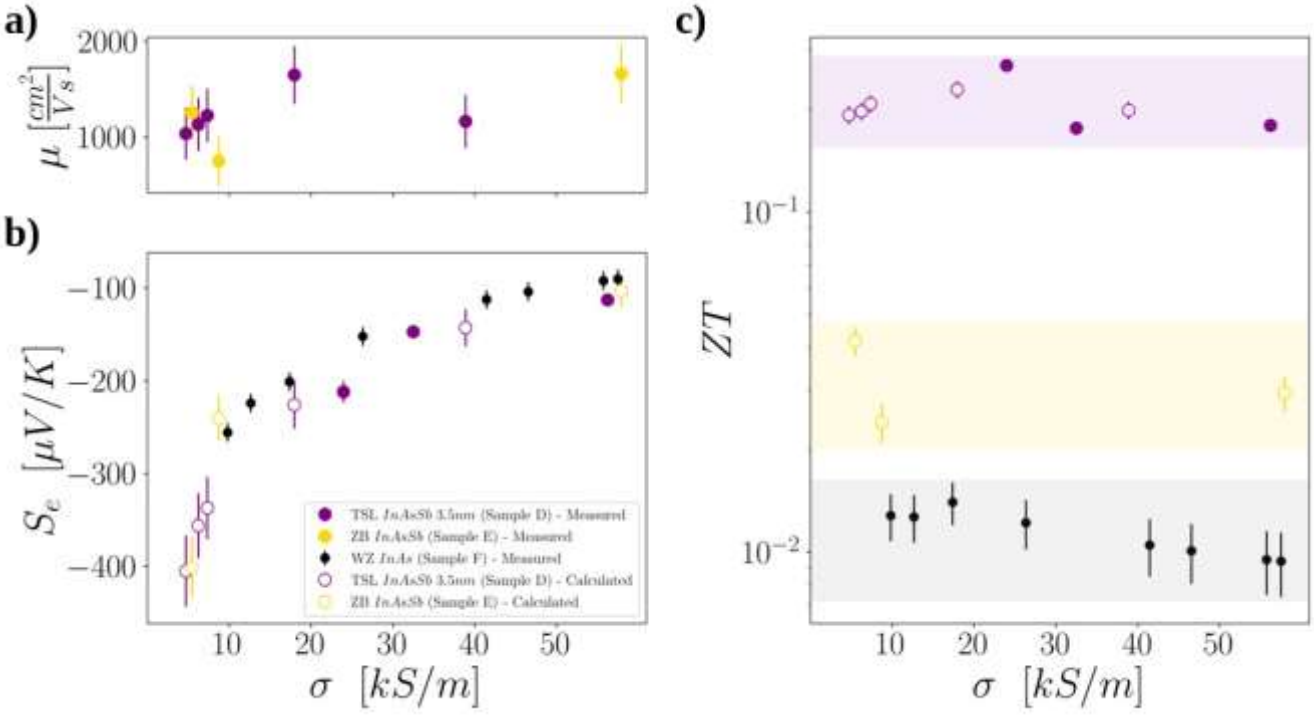

Figure 4. (a) Measured electron mobility of the NW-based FETs. As in all other panels, pure ZB InAsSb NWs are shown in yellow while violet indicates TSL InAsSb (3.5 nm). All the values are perfectly consistent, albeit slightly lower, with respect to electron mobility reported for pure WZ InAs NWs at room temperature [17, 18, 47]. (b) Seebeck coefficient extracted for samples D, E and F. Full (open) dots correspond to measured (calculated) data. (c) Thermoelectric figure of merit ZT for WZ InAs NWs (full black dots), ZB InAsSb NWs (open yellow dots) and twin superlattice InAsSb NWs with 3.5 nm periodicity (full and open violet dots).

CONCLUSIONS

We have unveiled experimentally for the first time the correlation between the controlled formation of periodical crystal defects (twins) in NWs and their thermal transport properties, demonstrating a decrease up to one order of magnitude in the thermal conductivity of TSL InAsSb NWs with respect to their pure ZB counterparts. We have reported TSL InAsSb NWs with average diameter of 70nm exhibiting thermal conductivity as low as $1.2\ \text{W/mK}$, that is, an order of magnitude lower than WZ InAs NWs with same diameter. This unprecedented decrease of thermal conductivity due to the occurrence of the twin superlattice was shown to coexist with unaltered electrical conductivity with respect to the InAs NWs, leading to a 10-fold increase in the ratio σ/κ. Besides, almost identical electron mobility and Seebeck coefficient were extracted for pure ZB and TSL InAsSb NWs, with values in agreement with WZ InAs NWs with similar diameters at room temperature. The giant reduction of k together with unaltered σ, μ and S overall lead to a thermoelectric figure of merit for TSL InAsSb NWs more than one order of magnitude higher with respect to WZ InAs NWs, with the highest reported value of $\text{ZT} = 0.24 \pm 0.07$ in III-V NWs. The generality of the twinning process, together with the possibility to engineer TSL NWs with different III-V and IV semiconductors, increase the impact of the present results making them a cornerstone for the development of a new generation of high-performance nanostructures for thermoelectric energy conversion.

METHODS

NWs growth. InAsSb NWs were grown on InAs(111)B substrates by Au-assisted Chemical Beam Epitaxy (CBE) in a Riber Compact-21 System. The system employs pressure control of the metalorganic (MO) precursors in the gas lines to vary the precursor flux on the sample during growth. The precursors used for

the NW growth were trimethylindium (TMIn), tertiarybutylarsine (TBAs), and tert-dimethylaminoantimony (TDMASb). Au nanoparticles (NPs) were obtained by drop-casting of colloidal solution onto the bare substrates. Colloids of 20 and 40 nm diameter were used. After degassing the substrates at 300°C, they were mounted into the CBE chamber and short InAs NW stems were grown using 0.6 Torr and 1.6 Torr of TMIn and TBAs line pressures respectively, at the substrate temperature of 400 ± 5°C. Then, to grow the InAsSb segments, the TMIn line pressure was changed to 0.9 Torr while TBAs and TDMASb line pressures were set to the values reported in Table 1, and the growth temperature was increased to 440°C within 5 min. The InAsSb growth proceeded at this temperature for further 50 minutes. At the end of the growth the TMIn flux was stopped, while the samples were cooled down under both TDMASb and TBAs flow. In Table 1 we summarize the growth parameters, the measured chemical composition and the crystal structure of the NWs.

NW morphology & structure characterization. The morphology of the NWs was characterized by means of scanning electron microscope (SEM) using a Zeiss Merlin field-emission microscope at an accelerating voltage of 5 keV. Chrystal structure and chemical composition of the InAsSb segment were analyzed by transmission electron microscopy (TEM) in a JEM-2200FS, equipped with in-column Ω filter and Oxford X-ray energy dispersive spectrometer (EDX), operated at 200 keV. Imaging was performed in high resolution (HR) TEM mode combined with zero-loss energy filtering and by high angle angular dark-field in scanning mode (HAADF-STEM) for the EDX measurements.

Device fabrication.
After the growth, the NWs were mechanically detached from the growth substrate by means of sonication and dispersed in isopropyl alcohol (IPA). The adopted fabrication protocol was different for the two investigated device architectures. For standard NW-based FETs, NWs were directly transferred to a pre-patterned $p^{++}Si/SiO_2$ substrate (0.5 mm Si, 280 nm SiO_2) by drop-casting a droplet of IPA/NWs solution onto the substrate. In the case of suspended nanowire-based devices for thermal conductivity measurement, a PMMA sacrificial layer was preliminarily spun onto the substrate, and the NWs were drop-casted on top of it. For both the architectures, contact electrodes were then patterned using standard e-beam techniques. After the development and prior to metal evaporation (Ti/Au, 10/100 nm), the NW contact areas were passivated using an ammonium polysulfide $(NH_4)_2S$-based solution to promote the formation of low-resistance ohmic contacts [48]. In the case of suspended NW-based devices, after liftoff, the sacrificial layer underneath the contacts was removed by means of conventional oxygen plasma dry etching. See also Supporting Information SI.2-3.

Finite Element Modeling.
In its simplest formulation, the 3ω method relates the third harmonic of the voltage drop across a NW to the injection current as [41] $V_{3\omega} = \left(\frac{4LRR'}{\pi^4 S\kappa}\right) I^3$. This result, however, is an approximation that results from truncating the Fourier series expressing $V_{3\omega}$, and it can be shown to hold only in nanostructures of high thermal conductivity. Considering the giant reduction of κobserved in TSL NWs, a simple application of the cubic model to our dataset would lead to an underestimate of the NW thermal conductivity.

To account for that, the data analysis has been performed via a Finite Element Model, which is able to account for the non-linearities in the transport equations caused by the drastically reduced κ [17,41,43], as evident from Figure 2. The NWs were modeled as hexagonal prisms, with height and base were measured form the SEM images and TEM images respectively.

Our FEM model solves the coupled physics problem of heat equation and the local version of Ohm's law to account for Joule's heating and the consequent local change in electrical resistivity. The current, voltage and temperature profiles are then computed via the FEniCS package [49], allowing us to extract $V_{3\omega}(I)$ for each value of injection current experimentally used. This method allows us to perform a least-squares fit on

the experimental data with the thermal conductivity as the only free parameter, from which we obtained the values of κ discussed in the main text. See also Supporting Information SI.1.

3ω measurement setup.

The experimental setup adopted for the 3ω measurements was reported in previous works [17,41]. A SR830 Lock-in amplifier is connected via a series injection resistor (100 $\mathrm{k}\Omega$) to one of the outer contacts of the device under test. The sine-out frequency is varied from device to device in a range from 7 Hz to 13 Hz. The other outer contact is grounded. The first and third harmonic of the voltage drop is picked-up across the two inner contacts by means of phase-locked measurements and are employed to evaluate the nanowire electrical and thermal conductivity, respectively.

REFERENCES

[1] G. J. Snyder, E. S. Toberer, Nature Materials 2008, 7, 2 105

[2] F. Sauter, Angewandte Chemie 1951, 63, 23-24 582.

[3] H. Callen, Thermodynamics and an Introduction to Thermostatistics, 2nd Edition, Wiley, 1991.

[4] Zhou, Y. M., Zhao, L.-D., Adv. Mater. 29, 1702676. (2017)

[5] Dresselhaus, M., Chen, G., Tang, M., Yang, R., Lee, H., Wang, D., Ren, Z., Fleurial, J.-P. and Gogna, P. Adv. Mater. (2007)

[6] Wenting Ji, Xiao-Lei Shi, Wei-Di Liu, Hualei Yuan, Kun Zheng, Biao Wan, Weixia Shen, Zhuangfei Zhang, Chao Fang, Qianqian Wang, Liangchao Chen, Yuewen Zhang, Xiaopeng Jia, Zhi-Gang Chen, Nano Energy, 2021, 87, 106171.

[7] M. Y. Swinkels, M. R. Van Delft, D. S. Oliveira, A. Cavalli, I. Zardo, R. W. Van Der Heijden, E. P. Bakkers, Nanotechnology 2015, 26, 38

[8] Hochbaum, A. I. et al. Nature 451 (2008).

[9] Boukai, A. I. et al. Nature 451 (2008).

[10] S. Elyamny, Nano Lett. 2020, 20, 7, 4748–4753

[11] X. Y. Mi, X. Yu, K. L. Yao, X. Huang, N. Yang, J. T. Lu, Nano Letters 2015, 15, 8 5229.

[12] D. Prete et al., Nano Lett. 2019, 19, 5, 3033–3039

[13] D. G. Cahill, S. K. Watson, R. O. Pohl, Physical Review B 1992, 46, 10 6131.

[14] R. Chen, J. Lee, W. Lee, D. Li, Chemical Reviews 2019, 119, 15 9260.

[15] J. R. Szczech, J. M. Higgins, S. Jin, Journal of Materials Chemistry 2011, 21, 12 4037.

[16] L. Yang et al., Science Advances, 7,20. (2021)

[17] D. Prete, E. Dimaggio, V. Demontis, V. Zannier, M. J. Rodriguez-Douton, L. Guazzelli, F. Beltram, L. Sorba, G. Pennelli, F. Rossella, Advanced Functional Materials 2021, 31, 37 2104175.

[18] S. Roddaro, D. Ercolani, M. A. Safeen, S. Suomalainen, F. Rossella, F. Giazotto, L. Sorba, F. Beltram, Nano Letters 2013, 13, 8 3638.

[19] D. Zabek, F. Morini, Thermal Science and Engineering Progress 2019, 9 235.

[20]. Y. Zhou, M. Hu, Nano Letters 2016, 16, 10 6178.

[21] A. Ghukasyan, R. LaPierre, Nanoscale, 2022,14, 6480-6487

[22] W. Li, X. Chen, Z. Zheng, Y. Chen, Computational Materials Science 2016, 112 107.

[23] M. De Luca, C. Fasolato, M. A. Verheijen, Y. Ren, M. Y. Swinkels, S. Kolling, E. P. Bakkers, R. Rurali, X. Cartoix, I. Zardo, Nano Letters 2019, 19, 7 4702.

[24] M. Xue, M. Li, Y. Huang, R. Chen, Y. Li, J. Wang, Y. Xing, J. Chen, H. Yan, H. Xu, J. Chen, Advanced Materials 2020, 32, 40.

[25] Y. He, G. Galli, Physical Review Letters 2012, 108, 21 215901.

[26] H. Dong, B. Wen, Y. Zhang, R. Melnik, RSC Advances 2017, 7, 48 29959.

[27] M. Hjort, S. Lehmann, J. Knutsson, A. A. Zakharov, Y. A. Du, S. Sakong, R. Timm, G. Nylund, E. Lundgren, P. Kratzer, K. A. Dick, A. Mikkelsen, ACS Nano 2014, 8, 12 12346.

[28] Z. Ikonic, G. P. Srivastava, J. C. Inkson, Solid State Communications 1993, 86, 12 799.

[29] A. G. Jackson, Handbook of Crystallography, Springer New York, 1991.

[30] Z. Ikonic, G. P. Srivastava, J. C. Inkson, Physical Review B 1995, 52, 19 14078.

[31] A. Porter, C. Tran, F. Sansoz, Physical Review B 2016, 93, 19 195431.

[32] N. I. Goktas, A. Sokolovskii, V.G. Dubrovskii, and R.R. LaPierre, Nano Letters 2020, 20,5,3344-3351.

[33] T. Xu, K.A. Dick, S. Plissard, T.H. Nguyen, Y. Makoudi, M. Berthe, J. P. Nys, X. Wallart, B. Grandidier, P. Caroff, Nanotechnology 2012, 23,095702.

[34] S. Xiong, Y. A. Kosevich, K. Saaskilahti, Y. Ni, S. Volz, Physical Review B - Condensed Matter and Materials Physics 2014, 90, 19

[35] R. E. Algra, M. A. Verheijen, M. T. Borgstrom, L. F. Feiner, G. Immink, W. J. Van Enckevort, E. Vlieg, E. P. Bakkers, Nature 2008, 456, 7220 369.

[36] P. Caroff, K. A. Dick, J. Johansson, M. E. Messing, K. Deppert, L. Samuelson, Nature Nanotechnology 2009, 4, 1 50.

[37] M. Cassinelli, S. Muller, K.-O. Voss, C. Trautmann, F. Volklein, J. Gooth, K. Nielsch, M. E. Toimil-Molares, Nanoscale 2017, 9 3169.

[38] D. Ercolani, M. Gemmi, L. Nasi, F. Rossi, M.Pea, A. Li, G. Salviati, F.Beltram, and L.Sorba, Nanotechnology 2012, 23,115606.

[39] A. Ghukasyan and R. LaPierre, Thermal transport in twinning superlattice and mixed-phase GaAs nanowires, Nanoscale, 2022, 14, 6480–6487

[40] Yingguang Liu et al, Utilizing twin interfaces to reduce lattice thermal conductivity of superlattice, International Journal of Heat and Mass Transfer, Volume 189, 2022, (https://doi.org/10.1016/j.ijheatmasstransfer.2022.122700).

[41] M. Rocci, V. Demontis, D. Prete, D. Ercolani, L. Sorba, F. Beltram, G. Pennelli, S. Roddaro, F. Rossella, Journal of Materials Engineering and Performance 2018, 27, 12 6299.

[42] L. Lu, W. Yi, D. L. Zhang, Review of Scientific Instruments 2001, 72, 7 2996.

[43] G. Pennelli, A. Nannini, M. Macucci, Journal of Applied Physics 2014, 115, 8.

[44] F. Zhou, A. L. Moore, J. Bolinsson, A. Persson, L. Froberg, M. T. Pettes, H. Kong, L. Rabenberg, P. Caroff, D. A. Stewart, N. Mingo, K. A. Dick, L. Samuelson, H. Linke, L. Shi, Physical Review B - Condensed Matter and Materials Physics 2011, 83, 20 1.

[45] M. Ohyama, Journal of the Physical Society of Japan 1967, 23, 3 522.

[46] Yazji et al, Nano Research 2015, 8(12): 4048–4060; old references 43 to 46 renumbered accordingly.

[47] D. Prete, V. Demontis, V. Zannier, M. J. Rodriguez-Douton, L. Guazzelli, F. Beltram, L. Sorba, F. Rossella, Nanotechnology 2021, 32, 14 145204.

[48] D. Suyatin, C. Thelander, M. Björk, I. Maximov, L.Samuelson, Nanotechnology 2007, 18, 105307.

[49] A. Logg, G.N. Wells, ACM Transactions on Mathematical Software, 2010, 37,2.